Development of a Coupled Land Surface and Groundwater Model

Reed M. Maxwell

Environmental Science Division, Lawrence Livermore National Laboratory, Livermore, California

Norman L. Miller

Earth Sciences Division, Lawrence Berkeley National Laboratory, Berkeley, California

ABSTRACT

Traditional land surface models (LSMs) used for numerical weather simulation, climate projection, and as inputs to water management decision support systems, do not treat the LSM lower boundary in a fully process-based fashion. LSMs have evolved from a leaky-bucket approximation to more sophisticated land surface water and energy budget models that typically have a specified bottom layer flux to depict the lowest model layer exchange with deeper aquifers. The LSM lower boundary is often assumed zero flux or the soil moisture content is set to a constant value; an approach that while mass conservative, ignores processes that can alter surface fluxes, runoff, and water quantity and quality. Conversely, groundwater models (GWMs) for saturated and unsaturated water flow, while addressing important features such as subsurface heterogeneity and three-dimensional flow, often have overly simplified upper boundary conditions that ignore soil heating, runoff, snow, and root-zone uptake. In the present study, a state-of-the-art LSM (Common Land Model) and a variably saturated GWM (ParFlow) have been coupled as a single-column model.

A set of simulations based on synthetic data and data from the Project for Intercomparison of Land-surface Parameterization Schemes (PILPS), version 2(d), 18-yr dataset from Valdai, Russia, demonstrate the temporal dynamics of this coupled modeling system. The soil moisture and water table depth simulated by the coupled model agree well with the Valdai observations. Differences in prediction between the coupled and uncoupled models demonstrate the effect of a dynamic water table on simulated watershed flow. Comparison of the coupled model predictions with observations indicates certain cold processes such as frozen soil and freeze/thaw processes have an important impact on predicted water table depth. Comparisons of soil moisture, latent heat, sensible heat, temperature, runoff, and predicted groundwater depth between the uncoupled and coupled models demonstrate the need for improved groundwater representation in land surface schemes.

1. Introduction

Early climate simulation models used a leaky-bucket parameterization to represent land surface hydrology as the lower boundary condition to atmospheric processes (Manabe et al. 1965). Such a simplistic description for land surface processes in global climate models (GCMs) led to the development of land surface models (LSMs) that include vegetation, surface resistance, and snow schemes that calculate time- and space-varying momentum, heat, and moisture fluxes to the lower atmosphere (e.g., Dickinson et al. 1986; Sellers et al. 1986). This was followed by LSMs with improved representations of subsurface hydrology, lateral soil moisture movement, evapotranspiration (Abromopoulos et al. 1988), and continental-scale river routing (Russell and Miller 1990). At about this time, regional climate modeling with similar LSMs began to provide higher spatial resolution (Dickinson et al. 1989; Giorgi 1990). These regional climate models are based on numerical weather prediction models coupled with global climate model LSMs. More recently, detailed descriptions of surface infiltration and lateral baseflow have been developed (Famiglieti and Wood 1991; Wood et al. 1992; Liang et al. 1994). The most recent LSMs (e.g., Foley et al. 1996; Bonan 1998; Dai and Zeng 1997; Walko et al. 2000; Oleson et al. 2004) have advanced to include more detailed ecological and biogeochemical processes.

However, most LSMs to date have a parameterization at the bottom layer that is either specified as a constant or a representation of the overlying moisture gradient. The water balance computed by land surface models can be much improved by inclusion of groundwater processes and the interactive flux between the

Corresponding author address: Reed M. Maxwell, Environmental Science Division, Lawrence Livermore National Laboratory (L-208), 7000 East Avenue, Livermore, CA 94550.
E-mail: maxwell5@llnl.gov

water table (WT) and the LSM lower layer. Conversely, traditional groundwater models have a simplified upper boundary condition that is externally specified and intended to represent fluxes of water related to processes such as infiltration and evapotranspiration. These fluxes are often simplified, uncoupled, and may be averaged in time and space, possibly missing key dynamics of important land surface processes.

The Biosphere–Atmosphere Transport Scheme (BATS) assumes a constant value of 4×10^{-4} mm s^{-1} downward flux at the lowest soil layer (Dickenson et al. 1993), and the Simple Biosphere scheme (SiB) has a parameterized downward flux as a function of gravity based on slope (Sellers et al. 1986). During the last several years, the linkage between the land surface hydrology and the deep groundwater aquifer has received increasing attention. Salvucci and Entekhabi (1995) evaluated surface and groundwater interactions with a steady-state statistical approach that showed significant shifts in evapotranspiration and runoff. Levine and Salvucci (1999) used a modified groundwater model to evaluate the saturated and unsaturated zones and found that recharge was closer to observations than an uncoupled LSM with simple lower boundary conditions. Liang et al. (2003) developed a one-dimensional dynamic groundwater parameterization as a function of WT depth for a land surface model. Results indicate that the lower LSM soil layer is wetter with this new parameterization that accounts for fluxes between the WT and this layer. This also results in higher baseflow, lower peak runoff, and decreased evapotranspiration. Yeh and Eltahir (2005) developed a lumped unconfined aquifer model interactively coupled to a land surface model with a similar approach to Liang et al. (2003).

Hence, the development of a physically based and dynamically coupled land surface groundwater model has been proposed. The dynamics of this formulation hinges on the interactions across the LSM soil column and a deep groundwater model (GWM). For example, as Pikul et al. (1974) demonstrated that a series of one-dimensional Richards' equation models coupled to the Boussinesq equation could accurately represent a groundwater hydrograph. The purpose for such a coupled LSM and GWM is to determine the sensitivity of the WT and deep groundwater processes to changing climate variables, the impact of the GWM on the LSM, and in turn the surface to atmosphere fluxes. Finally, a coupled LSM–GWM will help to better understand groundwater and surface water interactions at a range of scales and their effects on water quality. In the following section we present an approach toward developing a coupled LSM–GWM, followed by a discussion of simulation and results, and finally a summary and concluding remarks.

2. Approach

To understand the sensitivity of an LSM with the addition of a lower flux and deep groundwater model,

a state-of-the-art LSM and deep groundwater model were selected in this study. The LSM used here is the hybrid version Common Land Model (Dai et al. 2003) and the GWM is ParFlow (Ashby and Falgout 1996). The following two subsections provide brief descriptions of the Common Land Model and ParFlow.

a. The Common Land Model

The hybrid form of the Common Land Model (CLM) was developed as a multi-institutional code (Dai et al. 2003). It is based on land surface models developed by Dickinson et al. (1986), Dai and Zeng (1997), and Bonan (1998). Each grid tile may be partitioned into multiple subgrids that define land characterizations at fine spatial resolution while providing computational efficiency. Each grid can be subdivided into any number of subgrids that contain a single land-cover type, including areas with the dominant and secondary vegetation types, bare soil, wetlands, and lakes. An additional land surface type was incorporated within CLM to represent an urban environment that is highly impermeable. CLM has a single vegetation canopy layer, 10 unevenly spaced soil layers, and up to 5 snow layers. Vegetation processes are described as plant function types that are specified by optical, morphological, and physiological properties. The time-varying vegetation parameters include the stem and leaf area indices, and the fractional vegetation cover. CLM can be forced by observational atmospheric data or reanalysis data, or it can be fully coupled to an atmospheric model. CLM requires as input the atmospheric temperature (2 m), pressure, winds, precipitation rate, radiation (downward longwave, incident solar direct, and diffuse), and water vapor. The resulting prognostic variables are the temperature of the canopy, soil and snow layers, canopy water storage, snow depth, snow mass, snow water equivalent (SWE), and soil moisture content. CLM computes the momentum, latent heat, sensible heat, and ground heat fluxes, as well as the surface albedo and outgoing longwave radiation.

The water balance equations represent the link between the LSM and the GWM. The mass conservation equations are described in detail by Dai et al. (2003, 2001), and only a brief description of the soil moisture processes, and more importantly, the treatment of the lower soil water content formulation, is discussed here. The time rate of change in soil water content is defined as

$$\frac{\partial w_{\text{liq},j}}{\partial t} = [q_{j-1} - q_j] - f_{\text{root},j}E_{\text{tr}} + [M_{\text{il}}\Delta z]_j, \qquad (1a)$$

$$\frac{\partial w_{\text{ice},j}}{\partial t} = [q_{j-1,\text{ice}} - q_j] - f_{\text{root},j}E_{\text{tr}} + [M_{\text{il}}\Delta z]_j, \quad (1b)$$

where $w_{\text{liq},j} = (\rho_{\text{liq}}\theta_{\text{l}}\Delta z)_{\text{j}}$ and $w_{\text{ice},j} = (\rho_{\text{i}}\theta_{\text{i}}\Delta z)_{\text{j}}$ are the liquid and ice mass in each of the j soil layers; ρ is the density; θ is the volumetric soil moisture content; l is

liquid and i is ice; M_{il} is the ice to liquid phase change; q_j is the water mass flux at each layer interface; E_{tr} is the transpiration; $f_{root,j}$ is the root fraction for the j layer; and Δz is the vertical discretization of the soil column.

Soil water flux between layers is calculated in CLM by Darcy's law,

$$q = -K(\partial \psi / \partial z - 1), \quad (2)$$

where the hydraulic conductivity is given as $K = K_{sat}s^{2B+3}$ (Clapp and Hornberger 1978), the matric potential for unfrozen soil is given as $\psi = \psi_{sat}s^{-B}$, and by $\psi = 1000 [L_f(T_s - 273.16)/gT_s)]$ for frozen soil, where s is the fraction of saturation, $B = 2.91 + 0.159 \times$ percent clay [following the analysis in Cosby et al. (1984)], T_s is the surface soil temperature, L_f is the latent heat of fusion, and g is gravitational acceleration. The saturated hydraulic conductivity at depth (K_{sat}) is based on an exponential assumption,

$$K_{sat} = K_{sat,0} \exp(-z/z_L), \quad (3)$$

where $K_{sat,0}$ is the surface saturation hydraulic conductivity and z_L is the length scale for the decrease in K_{sat}.

Runoff in CLM is based only on basic concepts similar to the traditional TOPMODEL approach (Dai et al. 2001). Total runoff is the sum of the surface runoff (R_s) and baseflow (R_b), which are computed in CLM for saturated (f_{sat}) and unsaturated ($1 - f_{sat}$) regions separately:

$$R_s = (1 - f_{sat})\overline{w}_s^4 G_w + f_{sat}G_w, \quad (4a)$$

$$R_b = (1 - f_{sat})K_d\overline{w}_b^{(2B+3)} + f_{sat}10^{-5} \exp(-z_w), \quad (4b)$$

where G_w is the effective net liquid input (throughfall, dripping from leaves, snowmelt) to the upper soil layer; $\overline{w}_s$ and $\overline{w}_b$ are surface (upper three layers) and bottom (bottom five layers) soil thickness weighted soil wetness, respectively; f_{sat} is the fraction of the watershed that is saturated, given by

$$f_{sat} = w_{fact} \exp(-z_w), \quad (5a)$$

where w_{fact} is the fraction of the watershed having an exposed WT (a constant parameter related to the slope of the watershed). The mean, dimensionless WT depth, z_w is given by

$$z_w = f_z(z_{bot} - \sum_{j=1,nsoil} s_j\Delta z_j), \quad (5b)$$

where f_z is a WT depth scaling parameter (set to 1 m^{-1}) and z_{bot} is the depth of the bottom of the domain. Here K_d is the saturated hydraulic conductivity at the bottom layer. It is a calibrated parameter that allows for water balance closure as a residual calculation and is a focus of improvement here, as is the development of a flux term across the CLM lower boundary, infiltration, and the soil moisture time-evolving distribution, $\theta(t)_j$.

b. ParFlow

ParFlow is a groundwater flow code developed at Lawrence Livermore National Laboratory (Ashby and Falgout 1996). It solves two different sets of groundwater equations in two modes: 1) steady-state, fully saturated flow using a parallel, multigrid-preconditioned conjugate gradient solver or 2) transient, variably saturated flow using a parallel, globalized Newton method coupled to the multigrid-preconditioned linear solver. Both solution methods provide a very robust solution (i.e., computationally accurate and efficient) of pressure of water (hydraulic head) in the subsurface and excellent parallel scaling of solver performance (Ashby and Falgout 1996; Jones and Woodward 2001) and thus provide for solution of large (3D, with many computational nodes), subsurface flow systems with heterogeneous parameters. In the present study the transient, variably saturated mode (the second mode listed above) of ParFlow is used, and further discussion is limited to the processes and equations represented by this version of the model. Additionally, the examples presented here are in one-dimension, though future work will focus on multidimensions.

Parflow is an isothermal, variably saturated groundwater flow solver driven by external boundary conditions. It computes the pressure of the water in the subsurface and resulting saturation field over some change in time, given initial and boundary conditions (specified as pressure or flux of water). It does not account for frozen soil and ice processes, or any traditional land-surface-type processes such as runoff or evaporation, hence a motivation for the current work. ParFlow has a general representation of the subsurface; that is, there is no parameterization scheme involved in estimating the WT depth. The saturation field is calculated from the pressure field and a WT may be determined from the region where subsurface water pressure is greater than zero and saturation is 100%. Additionally, the size of the domain is not fixed and there are imposed rules for specifying subsurface parameters.

Parflow solves the mixed form of the Richards (1931) equation, given as

$$\frac{\partial[s(p)\rho\phi]}{\partial t} - \nabla\left[\frac{k(x)k_r(p)\rho}{\mu}(\nabla p - \rho g\nabla z)\right] = q, \quad (6)$$

where $s(p)$ is the water saturation for hydraulic pressure p, ρ is the water density, ϕ is the effective porosity of the medium, $k(x)$ is the absolute permeability of the medium, μ is the viscosity, $k_r(p)$ is the relative permeability, q represents any source terms, and z is the elevation. Both the saturation-pressure and relative permeability-saturation functions are represented by the van Genuchten (1980) relationships
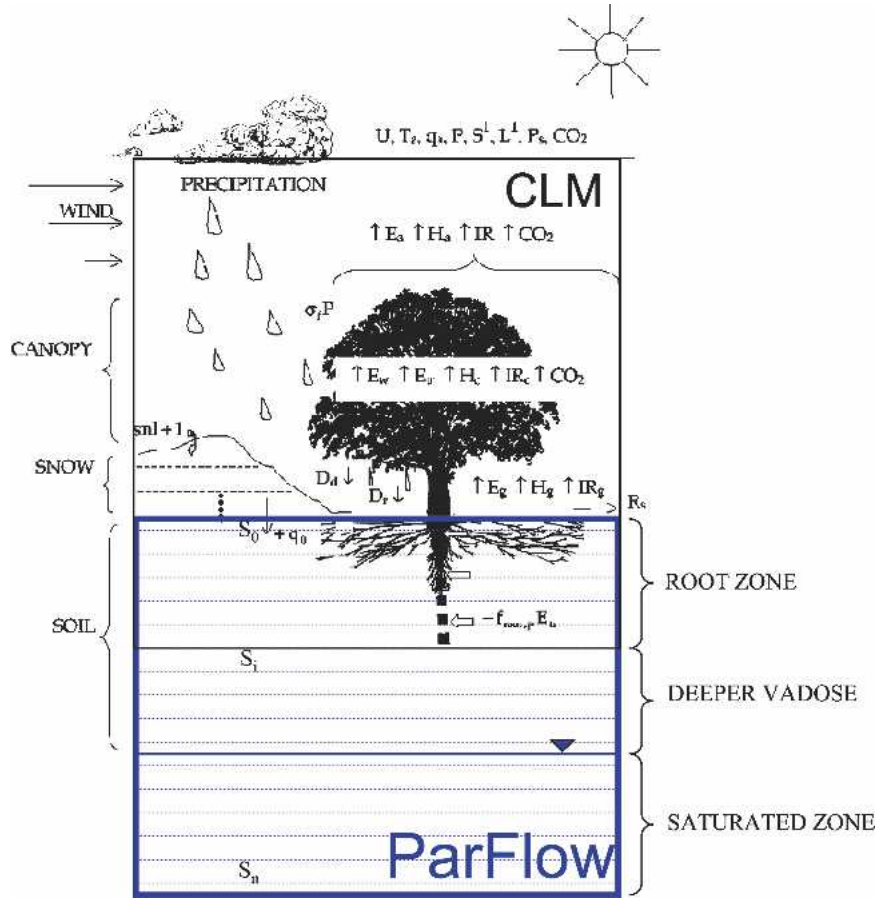
FIG. 1. Schematic of the coupled land surface–groundwater model. The lower box depicts the root zone, deeper vadose zone, and saturated zone represented by the ParFlow groundwater model. The upper box depicts the tree canopy, atmospheric forcing, and the land surface processes represented by CLM. Note the root zone, where the two models overlap and communicate.

$$s(p) = \frac{s_{\text{sat}} - s_{\text{res}}}{[1 + (\alpha p)^n]^{(1-1/n)}} + s_{\text{res}}, \qquad (7a)$$

$$k_r(p) = \frac{\left\{ 1 - \dfrac{(\alpha p)^{n-1}}{[1 + (\alpha p)^n]^{(1-1/n)}} \right\}}{[1 + (\alpha p)^n]^{(1-1/n)/2}}, \qquad (7b)$$

where α and n are soil parameters, s_{sat} is the saturated water content, and s_{res} is the residual saturation.

c. Coupled model CLM.PF

The CLM and ParFlow models were coupled at the land surface and soil column by replacing the soil column/root-zone soil moisture formulation in CLM with the ParFlow formulation. All processes within CLM, except for those predicting soil moisture, are preserved with the original CLM equations. The CLM simulation of soil moisture has been replaced by ParFlow's formu-

lation, resulting in a continuous hydrologic scheme, especially at the bottom layer of CLM.

A schematic of this coupled model (henceforth CLM.PF) is shown in Fig. 1, where the new soil moisture processes from ParFlow are outlined in blue. As this figure shows, these models overlap and communicate over the root zone. ParFlow soil moisture simulations are passed into CLM and infiltration, evaporation, and root uptake fluxes calculated by the CLM. These fluxes are passed to ParFlow where they are treated as water fluxes into or out of the model.

The two models communicate over the 10 soil layers in CLM with the uppermost cell layer in ParFlow corresponding to the first soil layer below the ground surface in CLM with the lateral ParFlow grid dimensions set equal to the size of tile in CLM. Equation (6) in ParFlow replaces Eq. (1a) in CLM, and the root-zone transpiration fluxes (F_{root}, $_jE_{\text{tr}}$) are still calculated by CLM and are represented in ParFlow by the general source term, q, in Eq. (6). As stated previously, Par-

Flow uses the van Genuchten relationships for relative permeability and saturation [Eqs. (7a) and (7b)], and these relationships replace the Clapp and Hornberger relationships used by CLM. Hydraulic properties are specified generally (not according to a land surface scheme) in ParFlow. The assumption that K_{sat} decreases exponentially with depth [Eq. (3)] is relaxed in CLM.PF, and K_{sat} may be specified based on site-specific conditions. Additionally, as ParFlow uses the van Genuchten relationships for soil moisture and relative permeability [Eqs. (7a) and (7b)], the relationships of Cosby et al. (1984) used in CLM to specify Clapp and Hornberger parameters are employed in CLM.PF.

The hydraulic pressure is calculated over the entire domain at a time step designated by the meteorological forcing (and specified by CLM and passed to ParFlow). Soil saturation is calculated from the hydraulic pressure solution [Eq. (7a)] over the entire domain, with the water content at the upper 10 layers passed back to CLM, where soil surface temperatures (T_s), heat fluxes, and energy balances are calculated. CLM still uses Eq. (1b) to determine the balance of ice in the soil column. The surface runoff and infiltration relationships are still calculated in CLM, using Eqs. (4) and (5). This preserves the infiltration-runoff partitioning model used by CLM; however the saturations given as input to Eqs. (5a) and (5b) are now calculated by ParFlow. The key differences between the coupled and uncoupled models are 1) the specification of soil and hydraulic parameters and 2) the calculation of the soil moisture profile. Differences in land-use cover would still be incorporated into CLM and may be reflected in the choice of soil properties. ParFlow is solved over the full CLM grid, including subgrids used to represent subgrid variability in land use.

The two models are dynamically coupled in a sequential manner with fluxes and variables communicated between models at every time step. A number of tests were performed to investigate the stability of the coupled processes, and the system was found to be quite stable with no need to iterate. The coupled model was found to be stable at time steps greater than 12 h, though typically shorter time steps are specified by the frequency of the external meteorological forcing.

3. Simulations and results

a. Initial simulations based on synthetic data

To test the coupled model (CLM.PF) and highlight the differences between CLM and CLM.PF, a simple simulation was undertaken designed to stress the two models. An imposed massive infiltration scenario was used. This scenario has specified 14 continuous days of steady rainfall at a rate of 0.01 mm s^{-1}, with no solar radiation. At the end of this 14-day interval the rainfall rate was set to zero and moderate incident solar radia-

tion (150 W m^{-2}) was simulated for 36 days. During the simulation, temperature, pressure and wind velocity were held constant at ambient conditions (T_s 300 K, p = 987.9 mb, and v = 0.6 m s^{-1}). The saturated hydraulic conductivity was set to K_{sat} = 0.361 (m day^{-1}) for both CLM and CLM.PF, and in an effort to set the subsurface properties as similarly as possible between the two models, z_L was set to 50 (m), and the van Genuchten parameters (n = 2 and α = 0.3 m^{-1}) were determined by fitting the van Genuchten profiles to the Clapp and Hornberger profile for B = 5.8. The modeled time step was 30 min.

Figures 2 and 3 show plots of the results of this simulation for CLM.PF and CLM, respectively. Two key forcing variables, precipitation and incident solar radiation, are plotted with runoff and infiltration, with the entire time series of the saturation profile plotted below in each figure. In both plots, time is displayed on a log scale. Note the subsurface depth is 2 m in CLM and 10 m in CLM.PF.

Infiltration starts almost immediately with the onset of precipitation and initially represents a large fraction of the surface water balance. Inspection of Fig. 2 clearly shows the infiltration response in CLM.PF on a logarithmic time scale, where a saturated infiltration front advances downward to the WT, shown in the figure as the region of water saturation equal to 100% that forms at the ground surface and expands downward. As the soil column fills with water, infiltration is moderated and runoff increases. At approximately 5 days the model has completely flooded and infiltration shuts off, and overland flow is the primary land surface flow process. Once the precipitation has ceased and incident solar radiation is turned on, the model slowly starts to dry out and by the end of the simulation period (48 days), the WT has slightly receded.

In Fig. 3 the very upper soil layer of CLM is seen to rapidly saturate within a few hours, causing saturation excess runoff to occur as a primary land surface flow process. The saturation front advances downward and reaches equilibrium within 10 days, but CLM does not flood. After the precipitation is turned off and incident solar radiation is imposed, CLM dries out, but much more rapidly than CLM.PF. Comparison of Figs. 2 and 3 highlights some of the land surface hydrologic process differences between the CLM and coupled CLM.PF models. This demonstrates that the addition of a deeper soil column with an explicit representation of the WT and saturated zone has a pronounced effect on the response of water in the soil column.

b. Comparison with observations at Usadievskiy Watershed, Valdai, Russia

To provide a more realistic comparison of the CLM and CLM.PF models, an observed 18-yr meteorological dataset from the Usadievskiy Watershed (henceforth Usad) in Valdai, Russia, was used (Robock et al. 1995; Vinnikov et al. 1996; Schlosser et al. 1997; Schlosser et
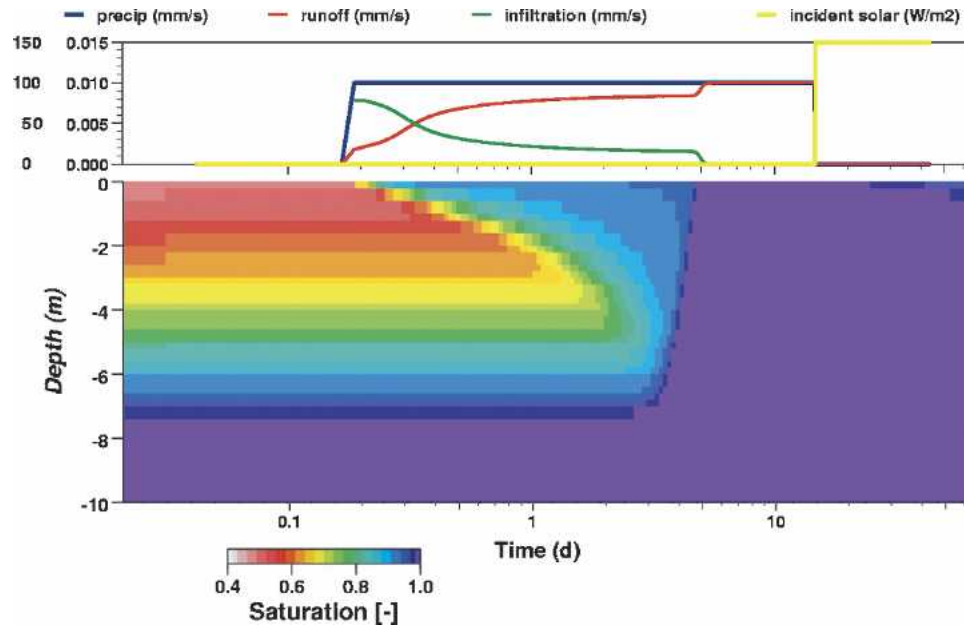
FIG. 2. Plot of meteorological forcing, precipitation, incident solar, and CLM.PF model results for runoff, infiltration, and soil saturation with depth as a function of time for the massive infiltration synthetic simulation. Note the log scale for time in this picture.

al. 2000; Slater et al. 2001; Luo et al. 2003). This dataset has been used extensively in cold-season studies within the Project for Intercomparison of Land-surface Parameterization Schemes (PILPS), version 2(d). It provides a very robust validation for models due to strong seasonal temperature variability ($\pm 50°$C), deep winter snowpack, a strong spring snowmelt and subsequent runoff, and a number of warm, summer precipitation events. For the current set of simulations the model parameters are given in Table 1. These parameters were derived from the International Geosphere–Biosphere Program (IGBP) soil classification for grassland and were modified based on all available observations at Valdai from Schlosser et al. (2000). The coupled model, CLM.PF, uses the van Genuchten relationships for saturation and relative permeability [Eqs. (6a) and (6b)]. The data given in Schlosser et al. (2000) are for Clapp and Hornberger soil parameters, so information regarding the van Genuchten parameters was needed. The data were obtained from Schaap and Leij (1998), based on an arithmetic average of soil parameters for the three descriptive soil types given in the soil-type composition at Valdai (loam 56%, sandy loam 28%, and sand 16%). A complete water balance of the Usad catchment is not available; however an estimate was performed in Schlosser et al. (1997). Based on an estimate of winter WT depth changes, deep percolation was simulated at a rate of 0.3 mm day^{-1}.
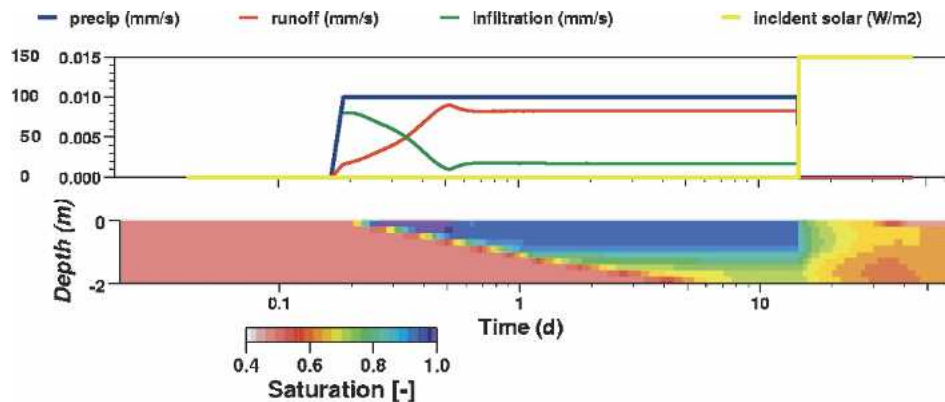

FIG. 3. Plot of meteorological forcing, precipitation, incident solar, and CLM model results for runoff, infiltration, and soil saturation with depth as a function of time for the massive infiltration simulation. Note the log scale for time in this picture.

TABLE 1. List of model parameters used in Valdai simulation.

	Parameter	Value	Units
α	Van Genuchten alpha	1.95	(m^{-1})
n	Van Genuchten exponent	1.74	
K_{sat}	Saturated hydraulic conductivity	1.21	(m day^{-1})
ϕ	Effective soil porosity	0.401	
s_{res}	Residual saturation	0.136	
w_{fact}	Fraction of model area with high WT	0.15	

All of the observations at the Usad catchment were made available by A. Robock and L. Luo as part of the Global Soil Moisture Databank (Robock et al. 2000; Luo et al. 2003), and all observations used for model comparisons come from these sources. Water table observations are not commonly compared to LSM simulations. Typically, LSM simulations include a quantity of water in a lower soil layer that may vary in a similar manner to WT depth (e.g., Fig. 10 of Schlosser et al. 1997). It is for this reason that simulation of WT depth is one of the motivations of the current coupled model and a focus of the results. The WT depth was recorded at many locations within the catchment (up to 20) and over a varying frequency, generally subweekly. These observations were spatially averaged to provide a catchment average of WT depth and are presented along with the minimum and maximum WT depth in the results below. Some of the more shallow wells were frozen during portions of the winter. An indication that a well was frozen was provided in the original data. These wells were screened (as were wells for which WT measurements were not available) from the calculation of catchment-averaged WT depth during those periods. As there were a large number of wells in the watershed, and typically fewer than one or two wells for any given measurement period were omitted, it was felt that this did not bias the results of the analysis.

There has been significant discussion (e.g., Yang et al. 1995) regarding the period of time a land surface model takes to come into thermal and hydrologic equilibrium from an initial set of conditions (i.e., model spinup). To insure proper model equilibrium a series of back-to-back 18-yr model runs were performed with the parameter values at the end of the first 18-yr simulation used as the initial condition for the second 18-yr simulation. This not only provided for model equilibrium but also provided information regarding model spinup time, which was between 1.5 and 2 yr.

1) COUPLED MODEL, CLM.PF, RESULTS, AND DISCUSSION

A portion of the results of the January 1966 to December 1983 simulation are presented in three plots, each with a 3-yr time series (Figs. 4a–c, 1969–71, 1972–74, and 1981–83), where the following quantities are presented:

(i) observed meteorological input forcing, daily averaged downward shortwave and longwave radiation, and reference temperature;

(ii) observed meteorological input forcing and monthly and daily cumulative precipitation;

(iii) monthly averaged runoff observations and model predictions;

(iv) minimum, maximum, and averaged water table observations plotted against daily averaged coupled model predictions;

(v) observations of snow water equivalent depth and model predictions; and

(vi) daily observations and model predictions of ground surface temperature.

In general the model results agree with the observations at the daily and monthly time scales (specific details follow).

From visual inspection of Fig. 4, the monthly averaged CLM.PF runoff (RO) simulations agree well with the timing and magnitude of the observations, with the best agreement occurring during the spring snowmelt runoff. The largest difference between the modeled and observed snowmelt peak runoff is in April 1972 [Fig. 4b(iii)]. Simulated daily averaged WT depth, SWE, and T_s also agree well with observations. For all four sets of simulations, the coupled model replicates observed daily variations and seasonal trends. Simulated WT depth is a new coupled model predictive measure that captures the summer variability and trends in observed WT depth. The WT depth observations are a site average of the 19 observation wells, and in all cases the model simulations fall within the minimum and maximum observed depths. The majority of the discrepancies between model simulations and observation occur during the winter months (e.g., December 1969 in Fig. 4a). The topography of the watershed is such that significant lateral flow in the subsurface would be expected. A one-dimensional column model cannot replicate this topography.

A suite of descriptive statistics was calculated for corresponding pairs of simulations and observations in time and is presented in Table 2. Following the recommendations in Willmott (1982), the average values for the observed and simulated ($\overline{O}, \overline{M}$) WT depth (meters), total monthly runoff (millimeters), SWE (millimeters), and T_s (degrees Celsius) along with the standard deviation of the observed and simulated values (s_o, s_m), the mean average error (MAE), the root-mean-square error (rmse) and the systematic and unsystematic root-mean-square error (rmse$_S$ and rmse$_U$), an index of agreement (d), the slope of a least squares linear regression (m), the sample coefficient of determination R^2, and the number of comparison pairs (N). The values listed for Table 2 are computed over the entire 18-yr simulation period, while Table 3 displays a subset of these comparison measures computed for each month, for WT depth.
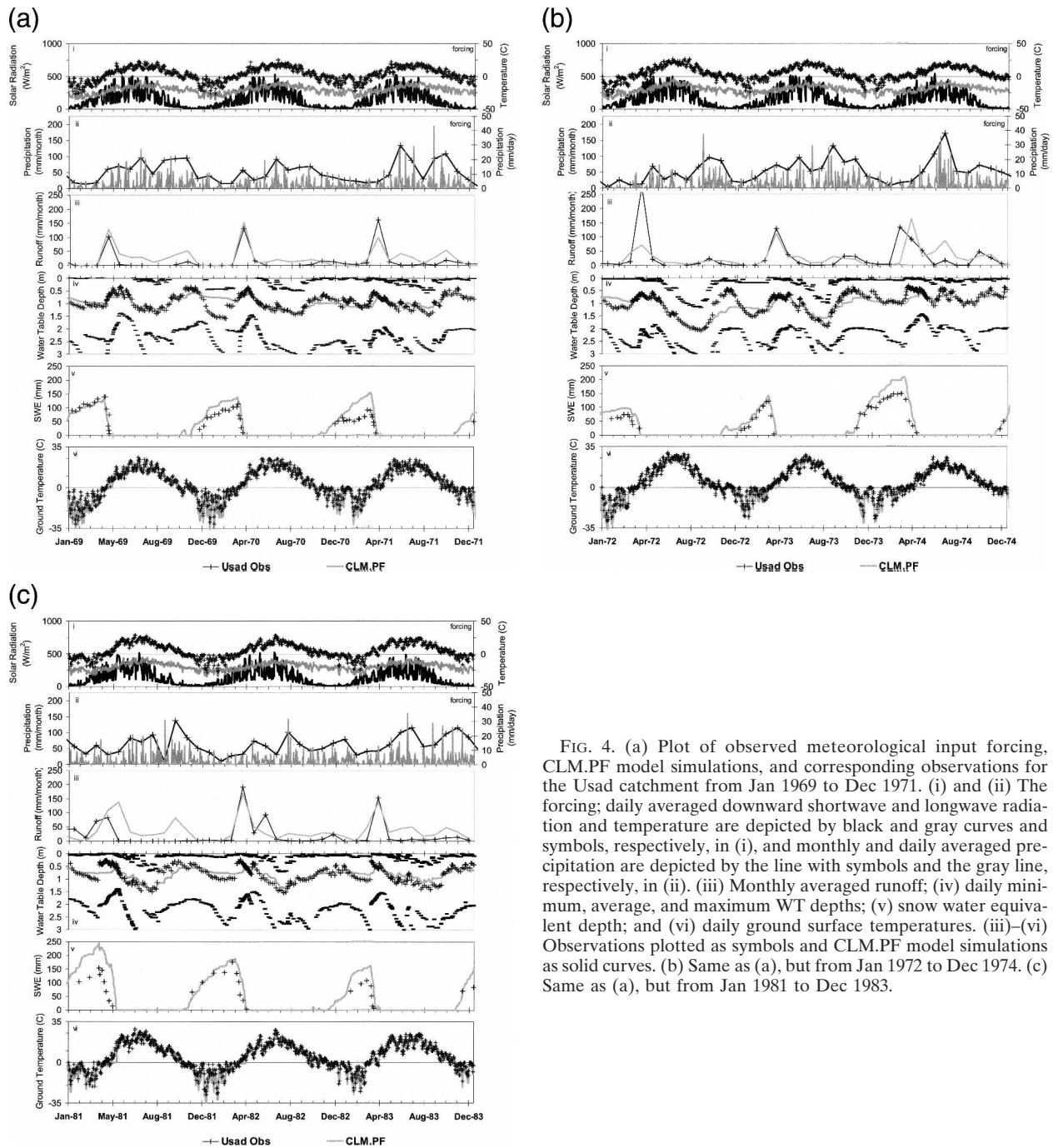
FIG. 4. (a) Plot of observed meteorological input forcing, CLM.PF model simulations, and corresponding observations for the Usad catchment from Jan 1969 to Dec 1971. (i) and (ii) The forcing; daily averaged downward shortwave and longwave radiation and temperature are depicted by black and gray curves and symbols, respectively, in (i), and monthly and daily averaged precipitation are depicted by the line with symbols and the gray line, respectively, in (ii). (iii) Monthly averaged runoff; (iv) daily minimum, average, and maximum WT depths; (v) snow water equivalent depth; and (vi) daily ground surface temperatures. (iii)–(vi) Observations plotted as symbols and CLM.PF model simulations as solid curves. (b) Same as (a), but from Jan 1972 to Dec 1974. (c) Same as (a), but from Jan 1981 to Dec 1983.

Overall, the descriptive statistics presented in Table 2 show agreement between model predictions and observations. The 18-yr averaged, simulated WT depth, RO and SWE ($\overline{M}$), overpredict the averaged observations ($\overline{O}$), with WT overpredicting by 8% and RO and SWE overpredicting by nearly 40%. On average, simulated T_s underpredicts the observations by 25%; T_s is the observation most accurately predicted by CLM.PF, with the highest d and R^2 values, while WT, RO, and

SWE are less accurately predicted by the model than T_s. The accuracy of predicted WT depth varies greatly during the year, as shown in Table 3. The statistics in Table 3 indicate that observed WT depth in May–November is much more accurately predicted by CLM.PF than December–April. Observed WT depths during the month of April are the least-accurately predicted by the model. It should be noted that the spatial variability in observed WT depth is always greater than

TABLE 2. Descriptive statistics of Usad observations (O) and model simulations (M). All quantities are in the units given (m, mm, and °C), except m, d, R^2, and N, which are unitless.

	$\overline{O}$	$\overline{M}$	s_o	s_m	MAE	Rmse	Rmse_S	Rmse_U	d	m	R^2	N
WT (m)	0.82	0.89	0.36	0.23	0.19	0.25	0.20	0.16	0.81	0.49	0.55	2451
RO (mm)	23	32	40	43	22	32	13	29	0.84	0.67	0.52	205
SWE (mm)	84	116	48	54	40	51	34	38	0.77	0.80	0.51	232
T_s (°C)	4.2	3.2	12.0	13.5	2.5	3.3	1.6	2.9	0.98	1.09	0.95	6574

the temporal variability in averaged WT depth over the catchment ($s_o = 0.9$ m for spatial compared to $s_o = 0.36$ for temporal).

Figure 5 presents a scattergram of daily observed and simulated WT depth for the entire 18-yr simulation period. Visual inspection of this plot again indicates an overall fair to good fit between observed and simulated WT depths. The scattergram is broken out into three subsets by T_s. The red dots, representing observed and simulated WT measurements for T_s greater than 5°C provide the best fit, indicating that warm-weather processes are well represented by the coupled model. For T_s below -5°C, the coupled model tends to underpredict the observed WT depths and for the freeze–thaw periods ($-5°$ to $+5°$C) the coupled model tends to overpredict observed WT depths. These results agree with the monthly statistics presented in Table 3.

As noted earlier, there is significant lateral subsurface flow at the Usad site. This lateral flow has the most significant effect on observed WT depths during the winter months, when the ground surface is frozen, snow covered, and hydraulically disconnected from the subsurface. Surface processes other than topography would have very little effect on the movement of the WT, and since infiltration and recharge are very low during the winter months the prime factor affecting water table levels would be redistribution due to gravity (e.g., Fig. 4b for January–February 1972). In this figure, temporal changes in average observed WT depth correspond with the minimum and maximum observed water table depth and the variability increases with time. The minimum observed water table depth is zero during this period, indicating discharge of groundwater at the ground surface. The variability in observed summer WT depth (Fig. 4b, 1972) stays relatively constant over time, and the fluctuations of the minimum, maximum, and average observed WT depth are in phase. Since the coupled model is operating in a single-column mode, it cannot capture the lateral movement of the WT during winter months and a distributed (2D surface, 3D subsurface) model would be needed to capture the variations in water table depth during winter months.

The less accurate WT simulations during freeze–thaw ($-5°$ to $+5°$C, inclusive) points to a different set of processes. Inspection of the dates corresponding to the points of poorest estimation in Fig. 5 (e.g., the green dots, up and to the left of the 45° dashed line) indicates they occur during the spring snowmelt that generally occurs during the month of April. An example of observed WT depth during a corresponding spring snowmelt is shown in Fig. 6, which presents observed and simulated runoff, WT depth, SWE, and T_s from February 1966 to June 1966. Careful inspection of Fig. 6 indicates a slight lag in the simulated 1966 spring thaw process. The simulated SWE is overestimated during this time, and there is a corresponding underestimation of the T_s as well. This underestimation of T_s and spring snowmelt causes the ground to remain frozen longer than observations, delaying the infiltration front that results from spring snowmelt. This same set of processes may be seen during the 1981 spring melt period (Fig. 4c). This feature does not appear to be related to the overestimation of midwinter SWE, as it is seen during the spring of 1966 (Fig. 6), which follows a winter where the SWE was not overestimated. This feature is not seen in some spring thaws—spring 1983, for ex-

TABLE 3. Descriptive statistics of Usad observations (O) and model simulations (M) of average WT depths aggregated by month. All quantities are in meters, except d and N, which are unitless.

| Month	$\overline{O}$	$\overline{M}$	s_o	s_m	MAE	Rmse	Rmse_S	Rmse_U	d	N
Jan	0.95	0.88	0.25	0.18	0.22	0.27	0.21	0.17	0.58	126
Feb	1.11	0.92	0.21	0.17	0.23	0.30	0.25	0.16	0.53	104
Mar	0.86	0.96	0.28	0.17	0.21	0.26	0.22	0.14	0.62	178
Apr	0.54	0.79	0.19	0.14	0.26	0.32	0.29	0.14	0.50	495
May	0.67	0.71	0.19	0.09	0.12	0.14	0.12	0.06	0.76	385
Jun	0.97	0.92	0.29	0.17	0.15	0.18	0.15	0.09	0.85	181
Jul	1.11	1.09	0.35	0.23	0.16	0.19	0.15	0.12	0.88	184
Aug	1.19	1.16	0.37	0.25	0.16	0.20	0.16	0.12	0.89	165
Sep	1.21	1.14	0.37	0.26	0.16	0.22	0.17	0.14	0.86	139
Oct	0.82	0.92	0.36	0.25	0.19	0.24	0.19	0.14	0.84	174
Nov	0.66	0.79	0.32	0.21	0.21	0.27	0.22	0.16	0.73	166
Dec	0.72	0.83	0.26	0.22	0.24	0.32	0.24	0.21	0.52	154
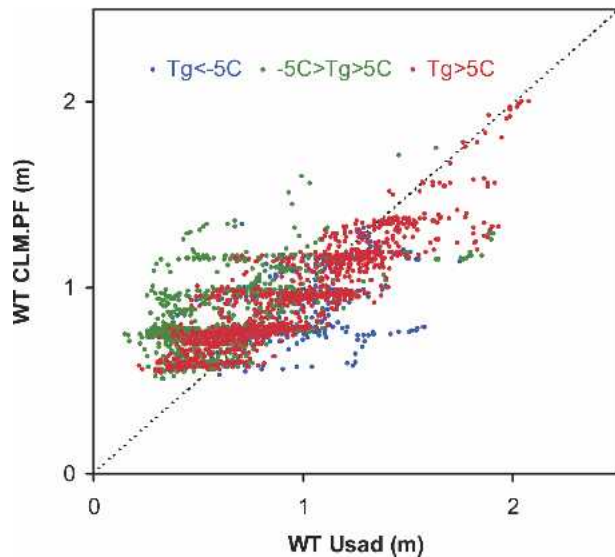
FIG. 5. Plot of observed vs simulated WT depth in meters. The three colors are separated out for ground surface temperatures below –5°C (blue, $m = 0.27$, $R^2 = 0.37$), from –5° to +5°C (green, $m = 0.27$, $R^2 = 0.28$), and greater than +5°C (red, $m = 0.64$, $R^2 = 0.80$).

ample (Fig. 4c)—where the timing of snowmelt and ground thaw agrees well with observations, resulting in good agreement of the WT simulations and observations.

Figure 7 further explores the simulation of T_s via a scattergram of observed and simulated daily averaged T_s, showing very good agreement between model simulations and observations, as also indicated by Table 2. There are some underestimations of daily averaged T_s with a maximum underestimation of 25°C, detailed on the figure by a dashed oval. Inspection of the dates of these underestimations reveals that they correspond to spring snowmelt and thaw periods, including the ones discussed above, primarily during the month of April. Comparison statistics similar to those presented for WT in Table 3 were also calculated for T_s. These statistics show CLM.PF did a poor job predicting observed T_s during the month of April, with all indicators of model performance being much lower than other months (e.g., 99% error in average, $d = 0.5$, $m = 0.35$, and $R^2 = 0.28$).

A further complication regarding the representation of cold processes in a 1D model is lateral spatial variability. Luo et al. (2003) noted lateral variability in the form of fractional snow coverage at the Usad site. This would lead to a different behavior than what is represented in the single-column model, where snow is either present at some depth or absent altogether. The 1D model is limited in its ability to represent situations where infiltration occurs at one location, due to snowmelt or rainfall, and not at other locations (where snow compaction or other processes might be taking place). This further substantiates the need to understand the affect of spatial variability on these processes.
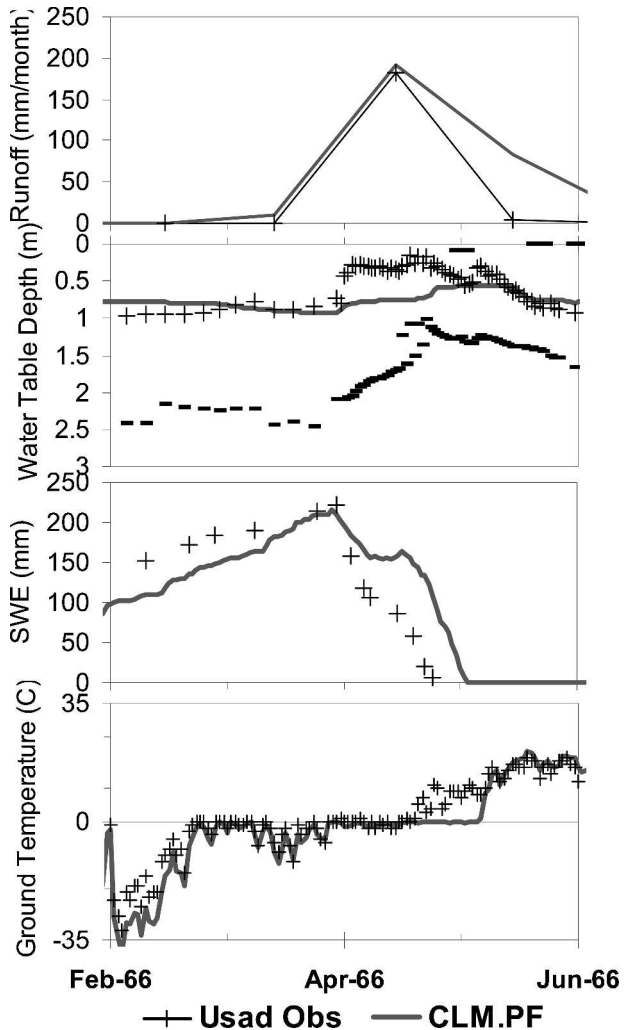

FIG. 6. Plot of observed and simulated runoff, groundwater depth, snow water equivalent depth, and ground surface temperature for the Usad catchment from Feb 1966 to Jun 1966. Observations are plotted as symbols, and CLM.PF model simulations are plotted as solid curves.

2) COMPARISON OF THE COUPLED AND UNCOUPLED MODELS, CLM.PF AND CLM, RESULTS AND DISCUSSION

Figure 8 presents a comparison of simulations for both the coupled (CLM.PF) and uncoupled (CLM) models compared to the Usad observations. In this figure, monthly averaged precipitation, runoff, sensible heat flux, and evapotranspiration are plotted. The simulations of sensible heat flux and evapotranspiration for the coupled and uncoupled models agree closely. The model simulations for runoff do include some differences, specifically during the periods of spring snowmelt. The timing of the spring snowmelt is similar for both the coupled and uncoupled models. However, the runoff rates are more accurately simulated by the coupled model, with the uncoupled model tending to
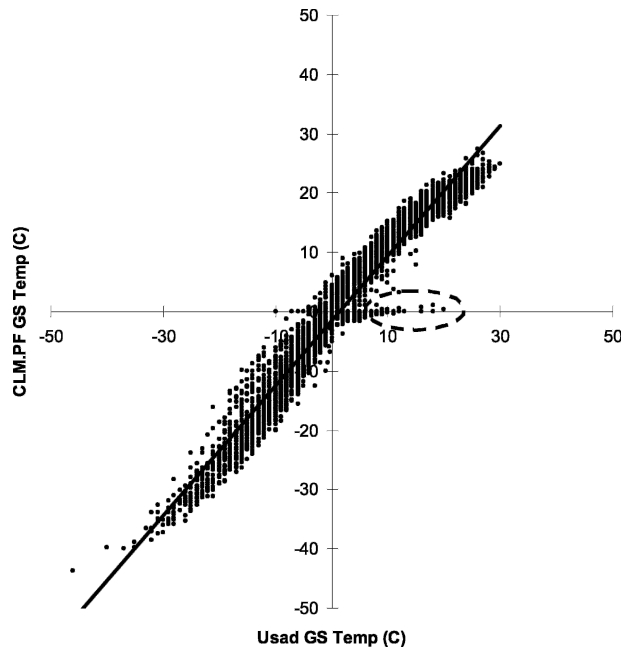
FIG. 7. Plot of daily averaged observed vs simulated ground surface temperature (°C), ($m = 1.1$, $R^2 = 0.95$).

underestimate the observed flow rate. The similarity in the two models' simulations of evapotranspiration would indicate a similarity in simulations of shallow soil moisture profiles. The differences in runoff would indicate a difference in simulations of deeper soil moisture as well as the effect of the explicit simulation of WT,

something present in the coupled model but absent in the uncoupled model.

Both the coupled and uncoupled models underpredict the evapotranspiration during summer months 1966 to 1972 (Figs. 8a and 8b), with 1972–73 (Fig. 8b) providing the best agreement between simulations and model observations. This underprediction, though significant in some years, falls within the range of evapotranspiration simulations reported by the PILPS 2(d) experiment. Figure 11a of Schlosser et al. (2000) plots the 21 model simulations to observed evapotranspiration at Usad. For example, the PILPS 2(d) model simulations range from 1.8 to 4.2 mm day^{-1} for June 1972 and 1.9 to 4 mm day^{-1} for July 1972; the CLM and CLM.PF model simulations (presented in Fig. 8b) are 2.7 mm day^{-1} for June 1973 and 3.3 mm day^{-1} for July 1973, and are close to the median among the range of model predictions.

Figures 9 and 10 investigate similarities and differences in simulated soil moisture between the CLM.PF, CLM, and observations. Figure 9 shows soil saturation plotted over depth and time for the observations, coupled, and uncoupled model simulations over the 18-yr simulation period. Figure 10 shows the same information for one year, 1973, to highlight temporal differences among the models. All three plots of soil saturation are plotted to a depth of 1 m, though the models simulated different total depths: 2 m for CLM and 6 m for CLM.PF. Comparison of these plots (Figs. 9 and 10) provides insight into the differences in model simulation and agreement with observations. Shallow simulations (20 cm) show that soil saturation for the coupled
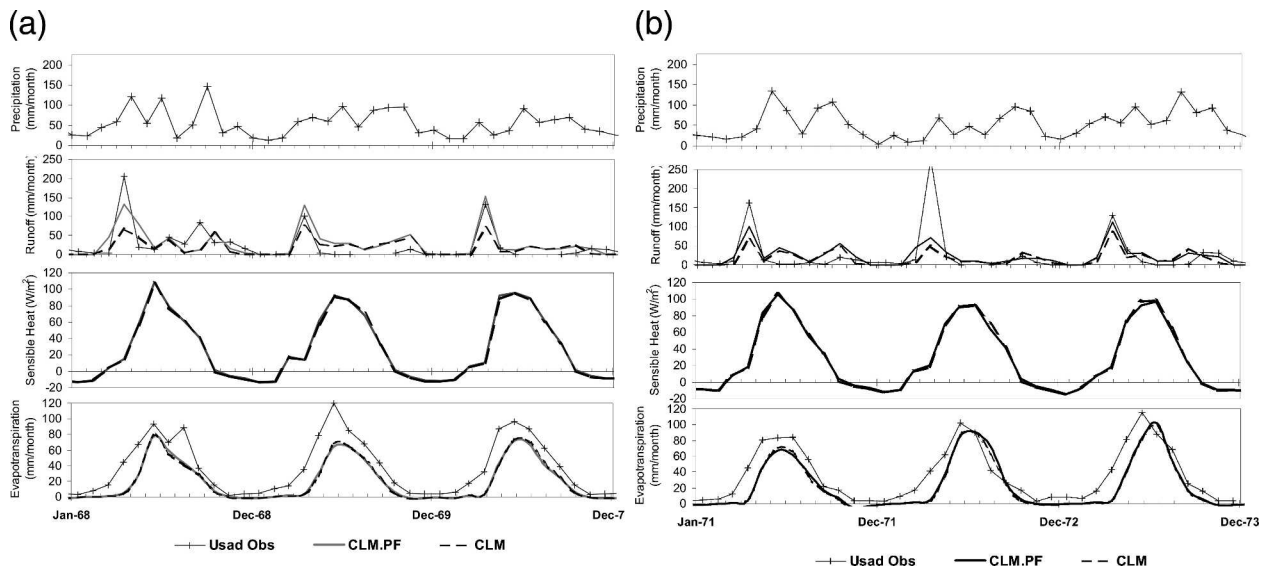

FIG. 8. (a) Plot of precipitation, runoff, sensible heat flux, and evapotranspiration for the Usad catchment from 1968 to 1970. Observations are plotted as symbols, CLM model simulations as dashed curves, and CLM.PF model simulations as solid curves. (b) Plot of precipitation, runoff, sensible heat flux, and evapotranspiration for the Usad catchment from 1971 to 1973. Observations are plotted as symbols, CLM model simulations as dashed curves, and CLM.PF model simulations as solid curves.
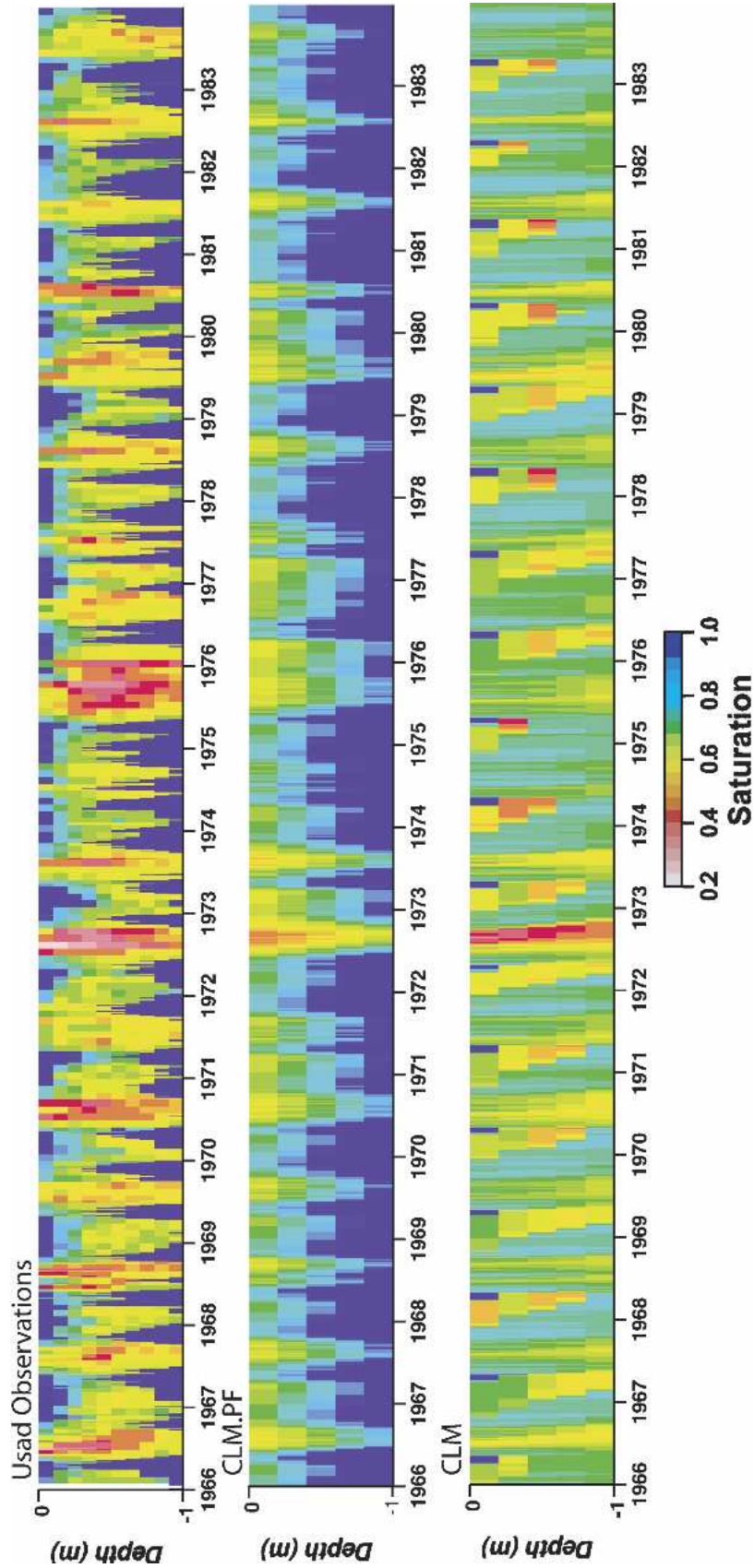
FIG. 9. Plot of observed and simulated soil saturations for Valdai as a function of time and depth over the entire 18-yr observation/simulation period. Average soil moisture observations for the (top) Usad catchment, (middle) CLM.PF model simulations, and (bottom) CLM simulations. Note that only the first 1 m of model simulations are plotted to match the observations. Note also that the solid blue regions denote completely saturated conditions where the WT depth is less than 1 m.
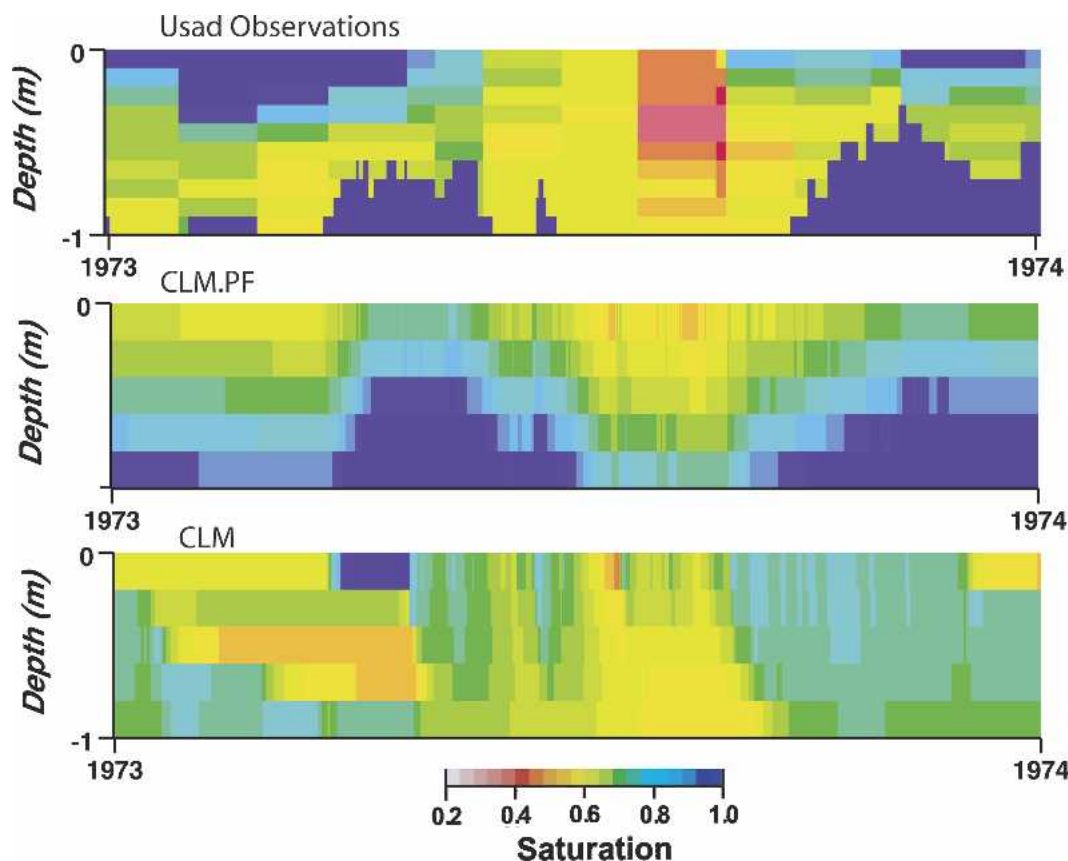
FIG. 10. Plot of observed and simulated soil saturations for Valdai as a function of time and depth for 1973. Average soil moisture observations for the (top) Usad catchment, (middle) CLM.PF model simulations, and (bottom) CLM simulations. Note that only the first 1 m of model simulations are plotted to match the observations. Note also that the solid blue regions denote completely saturated conditions where the WT depth is less than 1 m.

and uncoupled models are very similar, particularly during the summer months. This corresponds to the similarities in the simulated evapotranspiration between the two models. Deeper simulations of soil saturation (40 cm and greater) are quite different between the coupled and uncoupled models, with the coupled model simulations agreeing well with observations. The CLM parameterization of the subsurface, including the subsurface drainage and baseflow, is quite different than the parameterization used in CLM.PF. The uncoupled model also does not explicitly calculate a WT location, and these two factors contribute to differences in simulated soil moisture below 40 cm and to differences in simulated runoff and infiltration. CLM.PF stores water in the subsurface, which has an effect on model behavior beyond seasonal time cycles. This effect can be seen both in Figs. 8 and 9, where WT and soil moisture storage and memory affect other modeled processes.

4. Summary and conclusions

Coupling the land surface and groundwater models produces a model, CLM.PF, that behaves much differ-

ently than the previously uncoupled land surface model and expands the capabilities of the groundwater model to include land surface processes. This coupled model provides simulations of the subsurface, which, because of the explicit accounting for water up to and below the WT, have a memory of water stored in the deep subsurface. The simulations presented here show that this scheme balances mass across the land surface/groundwater boundary and provides new insights into coupled processes. The coupled model yields different behavior than the uncoupled model under flooding conditions, as seen in section 3a. The coupled model also has a different depiction of the root-zone soil moisture than the uncoupled model, leading to more realistic behavior that more closely matches observations at the Usad site [as discussed in section 3b(2)]. These differences stem solely from the soil saturations calculated by ParFlow and their impact on other calculated processes (e.g., runoff infiltration) in CLM.PF. The simulations of evapotranspiration are very similar between the coupled and uncoupled models [section 3b(2)], but simulations of runoff and soil moisture are improved in CLM.PF. The coupled model reproduces the averaged

observations for the Valdai wells [section 3b(1)], and some discrepancies in WT during periods of freeze/thaw have been demonstrated. There are also divergences in simulation between the coupled model and the Valdai data that warrant the need to investigate the affects of representing some processes and parameters (such as topography, subsurface heterogeneity, runoff, infiltration, and snow) in a distributed manner. Parameter uncertainty and spatial variability can be quite significant in surface and subsurface systems, and though it was not addressed in the current work and may affect outcomes, it should be considered in future studies. Nevertheless, the coupled model demonstrates the need for better groundwater representation in land surface schemes.

REFERENCES

Abromopoulos, F., C. Rosenzweig, and B. Choudhury, 1988: Improved ground hydrology calculations for global climate models (GCMs): Soil water movement and evaporation. *J. Climate,* **1,** 921–941.

Ashby, S. F., and R. D. Falgout, 1996: A parallel multigrid preconditioned conjugate grandient algorithm for groundwater flow simulations. *Nucl. Sci. Eng.,* **124,** 145–159.

Bonan, G. B., 1998: A Land Surface Model (LSM version 1.0) for ecological, hydrological, and atmospheric studies: Technical description and user's guide. NCAR Tech. Note NCAR/TN-417+STR.

Clapp, R. B., and G. M. Hornberger, 1978: Empirical equations for some soil hydraulic properties. *Water Resour. Res.,* **14,** 601–604.

Cosby, B. J., G. M. Hornberger, R. B. Clapp, and T. R. Ginn, 1984: A statistical exploration of the relationships of soil moisture characteristics to the physical properties of soils. *Water Resour. Res.,* **20,** 682–690.

Dai, Y. J., and Q.-C. Zeng, 1997: A land surface model (IA94) for climate studies. Part I: Formulation and validation in of-line experiments. *Adv. Atmos. Sci.,* **14,** 433–460.

——, X. Zeng, and R. E. Dickinson, 2001: The Common Land Model (CLM): Technical documentation and user's guide. 69 pp.

——, and Coauthors, 2003: The Common Land Model. *Bull. Amer. Meteor. Soc.,* **84,** 1013–1023.

Dickinson, R. E., P. J. Kennedy, A. Henderson-Sellers, and M. Wilson, 1986: Biosphere–Atmosphere Transport Scheme (BATS) for the NCAR Community Climate Model. NCAR Tech. Note NCAR/TN-275+STR, 69 pp.

——, R. M. Errico, F. Giorgi, and G. T. Bates, 1989: A regional climate model for the western U.S. *Climatic Change,* **15,** 383–422.

——, A. Henderson-Sellers, and P. J. Kennedy, 1993: Biosphere–Atmosphere Transport Scheme (BATS) version le as coupled to the NCAR Community Climate Model. NCAR Tech. Note NCAR/TN-387+STR, 72 pp.

Famiglieti, J. S., and E. F. Wood, 1991: Evapotranspiration and runoff from large land areas: Land surface hydrology for atmospheric general circulation models. *Surv. Geophys.,* **12,** 179–204.

Foley, J. A., C. I. Prentice, N. Ramankutty, S. Lewis, D. Pollard, S. Sitch, and A. Haxeltine, 1996: An integrated biosphere model of land surface processes, terrestrial carbon balance, and vegetation dynamics. *Global Biogeochem. Cycles,* **10,** 603–628.

Giorgi, F., 1990: Simulation of regional climate using a limited area model nested in a general circulation model. *J. Climate,* **3,** 941–963.

Jones, J. E., and C. S. Woodward, 2001: Newton-Krylov-multigrid solvers for large-scale, highly heterogeneous, variably saturated flow problems. *Adv. Water Resour.,* **24,** 763–774.

Liang, X., E. F. Wood, and D. P. Lettenmaier, 1994: A simple hydrolically-based model of land surface and energy fluxes for general circulation models. *J. Geophys. Res.,* **99,** 14 415–14 428.

——, Z. Xie, and M. Huang, 2003: A new parameterization for surface and groundwater interactions and its impact on water budgets with the variable infiltration capacity (VIC) land surface model. *J. Geophys. Res.,* **108,** 8613, doi:10.1029/2002JD003090.

Manabe, S., J. Smagorinsky, and R. F. Strickler, 1965: Simulated climatology of a general circulation model with a hydrologic cycle. *Mon. Wea. Rev.,* **93,** 769–798.

Levine, J. B., and G. D. Salvucci, 1999: Equilibrium analysis of groundwater–vadose zone interactions and the resulting spatial distribution of hydrologic fluxes across a Canadian prairie. *Water Resour. Res.,* **35,** 1369–1383.

Luo, L., and Coauthors, 2003: Effects of frozen soil on soil temperature, spring infiltration, and runoff: Results from the PILPS 2(d) experiment at Valdai, Russia. *J. Hydrometeor.,* **4,** 334–351.

Oleson, K. W., and Coauthors, 2004: Technical description of the Community Land Model (CLM), NCAR Tech. Note NCAR/TN-461+STR, 173 pp.

Pikul, M. F., R. L. Street, and I. Remson, 1974: A numerical model based on coupled one-dimensional Richards and Boussinesq equations. *Water Resour. Res.,* **10,** 295–302.

Richards, L. A., 1931: Capillary conduction of liquids through porous mediums. *Physics,* **1,** 318–333.

Robock, A., K. Ya. Vinnikov, C. A. Schlosser, N. A. Speranskaya, and Y. Xue, 1995: Use of midlatitude soil moisture and meteorological observations to validate soil moisture simulations with biosphere and bucket models. *J. Climate,* **8,** 15–35.

——, K. Y. Vinnikov, G. Srinivasan, J. K. Entin, S. E. Hollinger, N. A. Speranskaya, S. Liu, and A. Namkhai, 2000: The Global Soil Moisture Data Bank. *Bull. Amer. Meteor. Soc.,* **81,** 1281–1299.

Russell, G., and J. Miller, 1990: Global river runoff calculated from a global atmospheric general circuation model. *J. Hydrol.,* **117,** 241–254.

Salvucci, G. D., and D. Entekhabi, 1995: Hillslope and climatic controls on hydrologic fluxes. *Water Resour. Res.,* **31,** 1725–1739.

Schaap, M. G., and F. J. Leij, 1998: Database-related accuracy and uncertainty of pedotransfer functions. *Soil Sci.,* **163,** 765–779.

Schlosser, C. A., A. Robock, K. Ya. Vinnikov, N. A. Speranskaya, and Y. Xue, 1997: 18-year land surface hydrology model simulations for a midlatitude grassland catchment in Valdai, Russia. *Mon. Wea. Rev.,* **125,** 3279–3296.

——, and Coauthors, and the PILPS 2(d) Contributors, 2000: Simulations of a boreal grassland hydrology at Valdai, Russia, PILPS Phase 2(d). *Mon. Wea. Rev.,* **128,** 301–321.

Sellers, P. J., Y. Mintz, Y. C. Sud, and A. Dalcher, 1986: A simple

biosphere model (SiB) for use with general circulation mod–els. *J. Atmos. Sci.,* **43,** 505–531.

Slater, A. G., and Coauthors, 2001: The representation of snow in land surface schemes: Results from PILPS 2(d). *J. Hydrom-eteor.,* **2,** 7–25.

van Genuchten, M. Th., 1980: A closed form equation for pre–dicting the hydraulic conductivity of unsaturated soils. *Soil Sci. Soc. Amer. J.,* **44,** 892–898.

Vinnikov, K. Ya., A. Robock, N. A. Speranskaya, and C. A. Schlosser, 1996: Scales of temporal and spatial variability of midlatitude soil moisture. *J. Geophys. Res.,* **101,** 7163–7174.

Walko, R. L., and Coauthors, 2000: Coupled atmosphere–biophysics–hydrology models for environmental modeling. *J. Appl. Meteor.,* **39,** 931–944.

Willmott, C. J., 1982: Some comments on the evaluation of model performance. *Bull. Amer. Meteor. Soc.,* **63,** 1309–1313.

Wood, E. F., D. P. Lettenmaier, and V. G. Zartarian, 1992: A land-surface hydrology parameterization with subgrid vari–ability for general circulation models. *J. Geophys. Res.,* **97** (D3), 2717–2728.

Yang, Z.-L., R. E. Dickinson, A. Henderson-Sellers, and A. J. Pitman, 1995: Preliminary study of spin-up processes in land surface models with the first stage of Project for Intercom–parison of Land Surface Parameterization Schemes Phase 1(a). *J. Geophys. Res.,* **100,** 16 553–16 578.

Yeh, P. J.-F., and E. A. B. Eltahir, 2005: Representation of water table dynamics in a land-surface scheme. Part I: Model de–velopment. *J. Climate,* **18,** 1861–1880.